Advances in Science, Technology and Engineering Systems Journal Vol. 5, No. 6, 951-958 (2020)

www.astesj.com

Special Issue on Multidisciplinary Sciences and Engineering

ASTESJ

ISSN: 2415-6698

Investigating the Optical Behavior of Single/Multi-Dimensional Photonic Crystal Structures for Photovoltaic Applications

Gehad Ali Alsayed, Zahraa Ismail, Sameh O. Abdellatif *

FabLab, Centre for Emerging Learning Technologies (CELT) and Electrical Engineering Department, Faculty of Engineering, the British University in Egypt (BUE), Cairo, 11387, Egypt

ARTICLE INFO

Article history:
Received: 28 September, 2020
Accepted: 25 November, 2020
Online: 08 December, 2020

Keywords:
Third generation solar cells
Light trapping structures
Optical modeling
Distributed Bragg reflectors
Optimized Photonic crystals
Experimental fabrication
Optical Characterization

ABSTRACT

The results investigated in this work are toward the optimization of the photonic crystal structures in 1D and 2D scale. One-dimensional distributed Bragg reflectors (DBRs) have demonstrated substantial potential in various optoelectronic applications, due to the observed tunable optical band-gap. Herein, the use of DBRs in light trapping solar cells was simulated and validated, representing its effect as a back reflector structure. In terms of the layer thickness, material selection and number of layer, the optimized DBR structure was modeled and evaluated with respect to previously published numerical and experimental data. The proposed model is capable of designing photonic crystal structures with tunable band-gap varies from 400 nm to 700 nm while controlling the pass-band in both Visible and Near Infra-red regions. On the other hand, 2D grating structure has been simulated where the transmission spectra under various design dimensions have been investigated. Finally, thin film deposition is utilized for experimental validation to our proposed optical model.

1. Introduction

This paper is an extension of the work originally presented at the IEEE Conference on Power Electronics and Renewable Energy (CPERE) in 2019 [1].

Nowadays, new techniques of solar cells have shown a perfect solution to provide low cost alternative compared with conventional methods that used in solar cells [2-10]. These methods depend on using low cost active layer with less than 1 μm thickness and also minimizing the fabrication cost [2, 11-14]. By observing the literature, the reported structures showed low absorption in the active layer [15]. Based on that, the researchers began to find method to avoid the limitation in the absorption layer by using light trapping structures [8, 16, 17] (cf. Figure1). The light trapping structures can be divided into two main classifications, either by function or composition of the structure. The composition of the light trapping structure can be in the form of photonic crystal (PCs) [18] or plasmonics structures [1, 16, 17, 19-23]. The fabrication of PCs structures depends on the contrast between dielectric materials and semiconductor materials (refractive index contrast) which influences the optical properties of the structure [24]. This paper will discuss 1D PCs [25] as well as 2D grating structure for solar cells utilization

Additionally, other new generations of solar cells, namely dye sensitized solar cells and perovskites solar cells, showed enhanced performance with embedding two-dimensional colloidal crystal structures [26-29]. Such colloidal crystal structures are not only acting to enhance the photon capturing of the active layer of solar cells, but can be integrated for decorative purposes [29]. Over and above, light trapping techniques can have a positive role while harvesting diffused light in underwater applications [30, 31]

Light trapping structures can be applied in new technologies of solar cells, by trapping the light in the active layer through embedding nano-structures either above or below the active layer [8]. The technique of applying light trapping in the active layer depends on minimizing the reflected light in the upper layer by using anti-reflecting coating (ARC) while maximizing the reflected light in the back layer. The angle of reflection in the back reflector must exceed the critical angle, targeting total internal reflection in the active layer, which attributes to the absorption [8] (see Figure 1).

Additionally, other new generations of solar cells, namely dye sensitized solar cells and perovskites solar cells, showed enhanced

*Corresponding Author: Sameh O. Abdellatif, British University in Egypt (BUE), Cairo, 11387, Egypt, +201222194077, sameh.osama@bue.edu.eg

performance with embedding two-dimensional colloidal crystal structures [26-29]. Such colloidal crystal structures are not only acting to enhance the photon capturing of the active layer of solar cells, but can be integrated for decorative purposes [29]. Over and above, light trapping techniques can have a positive role while harvesting diffused light in underwater applications [30, 31].

The demonstrated optical model introduces an advanced optimization tool for 1D/2D PCs, seeking for maximum absorption in the active layer utilized in new generation of solar cells. Using Matlab scripting, the developed tool was essentially deployed and proved using a free optical simulator platform called "Open-Filter" [32], while absorption profiles were simulated numerically using Comsol multi-physics. The optimization procedure was applied on particular parameters such as the number of layers constricting the PC structure, the difference in refractive index and the layer thickness. The output results showed complete consistency with the literature data previously measured [20] and simulated [8, 17].

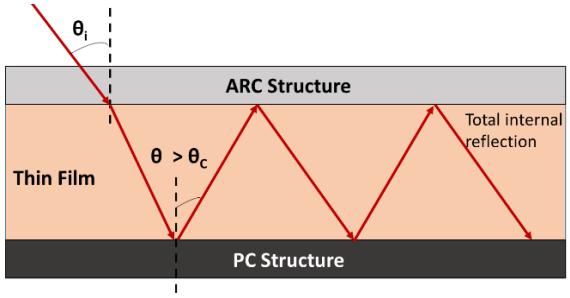

Figure 1: Schematic diagram of sandwiched light trapping structure for solar cells.

2. Optimization Model

2.1. Analytical modeling

The thin film optical modeling represented by characteristics matrix analytical method [33] is utilized in this paper. This method depends on Maxwell's equations which describe by electric field that cross continuously from medium to another. When the incidence of layer was given by electric and magnetic field, the field of both electric and magnetic can derived by matrix that given above [33]:

$$\begin{bmatrix} E_1 \\ H_1 \end{bmatrix} = M \begin{bmatrix} E_2 \\ H_2 \end{bmatrix} \quad (1)$$

where the intensity of electric and magnetic fields in the input medium are E_1 and H_1, while the electric and magnetic fields in the output medium are E_2 and H_2. Herein, M is given by:

$$M = \begin{bmatrix} \cos k_o h & i \sin k_o h/\gamma_1 \\ \gamma_1 i \sin k_o h & \cos k_o h \end{bmatrix} \quad (2)$$

and γ_1 is given by:

$$\gamma_1 = \sqrt{\frac{\varepsilon_o}{\mu_o}} \frac{n_1}{\cos \theta_i} \quad (3)$$

where h is thickness of thin film, k_o represented as propagation coefficient ($k_o = 2\pi/\lambda$), ε_o and μ_o are represented as air permittivity and permeability, refractive index of material called n_1, angle of incidence called θ_i.

A concatenation of layers can be referred to as a system matrix, represented by the multiplication of individual layer matrices. This matrix used to calculate the overall coefficients of reflection and transmission. Open-filters [32] is used as open source of analytic thin film optical modeling where we can validate our characterization matrix results.

Distributed Bragg Reflector (DBR) is a one-dimensional structure of simple photonic crystal. Optical band-gap is formed for Distributed Bragg Reflector as observed by solving Maxwell's equation (more detailed analytical solution for 1D and 2D photonic crystals can be accessed in [16]). The angle of incident and polarization should directly affect the width of band-gap. By incrementing the incidence angle to oblique, the TE modes band-gap becomes wider, while the band-gap of TM mode becomes narrower. This finding leads us to the independence of the band-gap from the polarizations and angle of incidence, as presented later in the discussion section. The photonic band-gap would exist, when contrast of dielectric occurred. In this manner, DBR could be shaped by layers of silicon with thickness 550 nm (n = 3.48) and SiO_2 of thickness 550 nm (n =1.46). The Lorentzian-Drude (LD) model introduced in [9] is used, which explain the absorption and dispersion of silicon as a wavelength dependent function.

2.2. Material modeling

The coefficient of dispersion should be calculated to modal dispersive and absorptive materials. Herein, Lorentzian-Drude (LD) model through FDTD simulations are enrolled [34]. The LD modal divided into two models. The Drude model is defined as the first model that, due to intra-band transitions, directly affects background absorption and dispersion. The second modal that represents dispersive media by multiplying resonant frequencies is the Lorentz model.

The model of semi-quantum reflects the electronic inter-band transitions. A material using the LD model's complex permittivity could be expressed by:

$$\varepsilon(\omega) = \varepsilon_{\bowtie} + \sum_n \frac{\sigma_n \omega_n^2}{\omega_n^2 - \omega^2 - i\omega\Gamma_n} \quad (4)$$

where $\varepsilon_{\bowtie}$ is the instantaneous dielectric response (DC), Γ_n and ω_n are the LD coefficients and σ_n is a position function that defines the power of the n^{th} resonance. Figure 2 shows the optical model for the DBR structure to be optimized. The optimization process is considering the number of DBR layers, reflective index (n_1– n_2), and the thickness of the layer (h_1, h_2).

2.3. Structure optical modeling using FDTD

The finite difference time-domain (FDTD) algorithm is used to make simulation of light interaction with various structure of layers [35]. The (FDTD) algorithm is considered as a standard numerical technique in classical electromagnetism. To simulate (FDTD) algorithm, open source algorithm is used called MEEP [36].The simulated volume is reflected on the required simulation time and RAM that required to make simulation on MEEP. A runtime of nearly 10 ns per pixel per time step of time is needed with RAM of almost 100 bytes per pixel [37].

MEEP was used to implement simulation of reflection and transmission of light by using different structure of light trapping. 10 μm × 10 μm is volume that used in simulation with unit step and resolution of 10 nm and 10 respectively. The wavelength is set as 550 nm to simulate sun irradiance for TM and TE modes. Figure 3, shows the modal with two detectors integrated for the calculation of transmitted and reflected field.

The maximum intensity of AM1.5G is determined to be 1000 W/m^2. Two identical Gaussian light sources with a width from 200 nm to 1500 nm and a mean wavelength of 550 nm, were utilized to represent TE and TM modes. It is important to model and integrate in MEEP the wavelength dependent variation in the real and imaginary parts of the refractive index for different materials used. Here, we integrate the published LD model to illustrate the complex refractive indices using the Lorentzian-Drude (LD) coefficients for the chosen materials with specific focus on Si as a semiconductor material. The compatibility of the LD model with MEEP is considered as the main reason for selecting it [38].

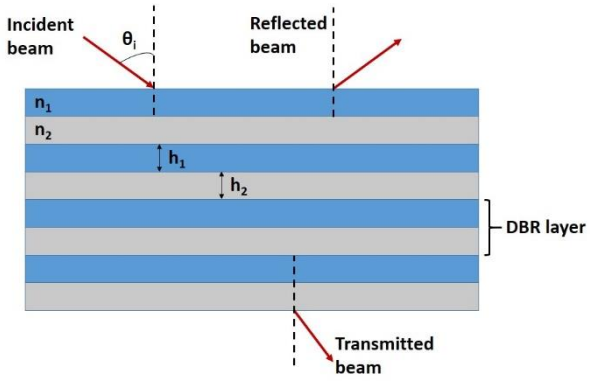

Figure 2: Schematic diagram of the structure of the DBR under test.

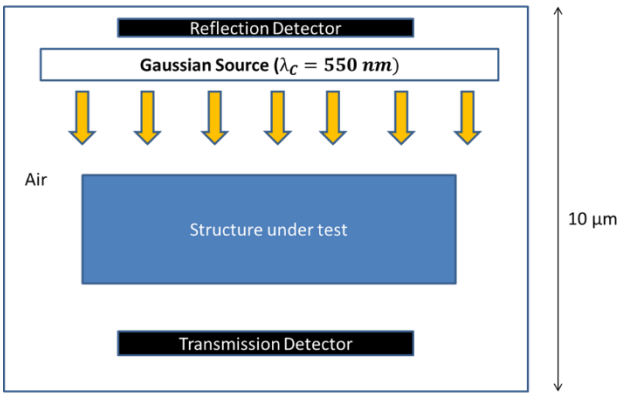

Figure 3: Schematic diagram used for the calculation of transmission and reflection spectra for the MEEP model.

2.4. 2D optical modeling using Comsol Multi-physics

Using the commercial simulator Comsol Multiphysics 5.0 [37], optoelectronic modeling is carried out. Comsol utilize finite element method (FEM) solver such that a tetrahedral mesh is selected based on the minimum feature length in the geometry under investigation. Various 2D optical structures devices could be simulated by optical and electromagnetic libraries and are modeled by the continuity, Poisson, drift-diffusion and Maxwell's equations assuming 2D solution. The targeted solar cells with light trapping structure are described as a p-i-n junction [39]. Consideration is also provided to the bulk, surface recombination, and contact effects. The primary governing equations are given by [8]:

$$-\nabla.\left(\frac{\varepsilon_o \varepsilon_r}{q}\nabla V\right) = -n + p + N_D(1 - f_D) - N_A(f_A) + \sum_j N_{tj}(\delta_j - f_{tj}) \quad (5)$$

$$\nabla.J_n - \sum_j R_n^{tj} - R_{sp} - R_{st} - R_{av} + G_{opt}(t) = \frac{\partial n}{\partial t} + N_D\frac{\partial f_D}{\partial t} \quad (6)$$

$$\nabla.J_p - \sum_j R_p^{tj} - R_{sp} - R_{st} - R_{av} + G_{opt}(t) = \frac{\partial p}{\partial t} + N_A\frac{\partial f_A}{\partial t} \quad (7)$$

where p and n are the excess hole concentration and minority-electron concentration with respect to equilibrium, N_A and N_D are the doping levels of acceptors and donors, J_p and J_n are the current density for holes and electrons, R_p and R_n represent the bulk recombination of holes and electrons, G_{opt} is the term for optical generation, R_{sp} represents the recombination of surfaces, and R_{av} and R_{st} are trapping recombination. The required optoelectronic parameters per each layer are captured from the simulation tool library and the optical generation term is calculated using an Matlab based optical model, taking into confederation a doping level of 10^{18} cm^{-3} in both the n and p sides [10].

Herein, the optical generation parameter G_{opt} plays a critical role in investigating the optical impact of the proposed photons management structure in enhancing the performance of the solar cell. The expected enhancement can be attributed to the elongation of the optical path length inside the active materials under simulation. This elongation is directly reflected on the generation term.

3. Simulation Results

3.1. Optimizing number of layer in DBR structure

Si-SiO$_2$ DBR structures have been simulated following the characteristics matrix analytical approach defined in the section two. Based on our previous work, these DBR structures were taken into account as an initial model to be optimized [8]. Firstly, the influence of the DBR layers on the presence of the optical band-gap was originally discussed in Figure 4. The spectra showing the reflectance are plotted and the structures of two, four and six DBR layers have been simulated. Here, the ratio between the the reflected light and the incident light is termed as the optical reflectivity (dimensionless unit), cf. Figures 2 and 3.

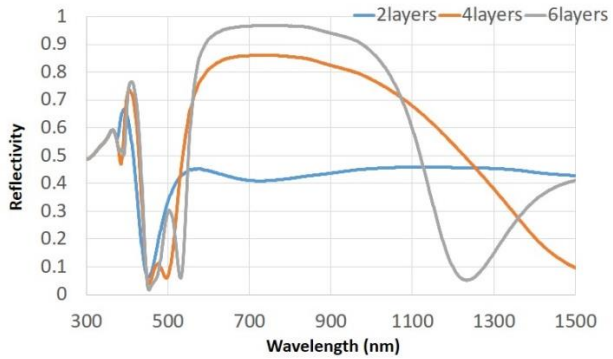

Figure 4: Si-SiO2 Reflectivity of DBR for different layer numbers.

It is evident from Figure 4 that the occurrence of the optical band-gap is associated to the number of layers constructing the one dimensional photonic crystal structure. 550 nm optical band-gap

(from 550 nm to 1100 nm) was formed with reflectively of around 0.95, while utilizing six DBR layers structures. In contrast, attention should be given to the trade in parameters concerned to the overall DBR dimensions and to the fabrication procedure sophistications. For instance, a sharper optical band-gap is anticipated by increasing the number of layers, more than six, however the complicity and fabrication cost will increase as well. Thus, the optimal structure in terms of layer count for such Si-SiO_2 DBR structure is the six layer DBR structure. It is worth noting that this layer number is not a global optimum, as the observation of the optical band-gap depends not only on the DBR layers count, but also plays the refractive index contrast plays an critical role.

3.2. DBR thickness optimization

Following the first optimization stage demonstrated in section 3.1, Figure 5 shows the influence of the thickness variance on reflectivity. The DBR structure of six layers optimized in section 3.1 is used. To reduce the variables included in the optimization problem under investigation, the thickness of both layers, SiO_2 and Si, are considered equal. Figure 5 examined 550 nm, 250 nm, and 125 nm reflectivity spectra. The nominated wavelengths are selected to fit the peak wavelength for the input source at 550 nm. Consequently, λ_o , $\lambda_o/2$ and $\lambda_o/4$ thicknesses have been simulated. As shown in Figure 4, the presence of the photonic-gap is associated at thin film thickness of $\lambda_o/4$. This is attributed to the maximum local point at which the maximum reflection occurs. The thin film thickness is nominated to be a 1/4 of the optical wavelength where maximum reflection is observed [14]. In view of the projection of a quarter wavelength layer of Si with a refractive index of n_1 and light on a wavelength layer of λ_o, the thickness h_1, which induces maximum reflection, is determined by [14]:

$$h_1 = \frac{\lambda_o}{4\, n_1} \quad (8)$$

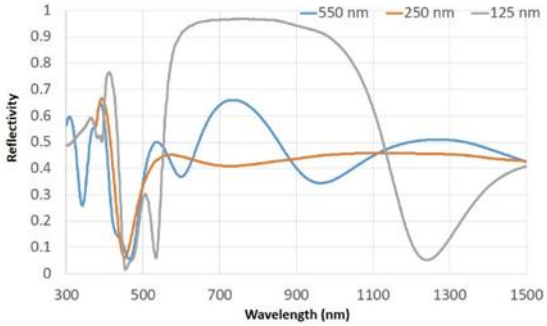

Figure 5: Six Si-SiO2 DBR reflectivity layers with various layer thicknesses.

3.3. Refractive index contrast optimization

Finally, Titanium dioxide is integrated as a direct substitution for Si, in order to examine the impact of refractive index contrast variation on the photonic-gap. TiO_2 is chosen as an easily prepared, low-cost and efficient n-type semiconductor material, knowing that we have already investigated its refractive index experimentally in [28]. Manual as well as automated Dr Blade screen printing can be utilized, as a sol-gel method, to deposit thin film of TiO_2 layer in micrometer range as previously discussed in [28]. In such context, diluted paste with isopropanol can be managed to tune the thin film thickness [27]. The large variation between the refractive index of TiO_2, nearly 1.78, and that of Si, around 3.9 [26], negatively contribute to the detected width of the band-gap. This narrowing can be observed in Figure 6, as a reduced, less sharp optical band-gap with maintaining the number of layers in both DBRs under test.

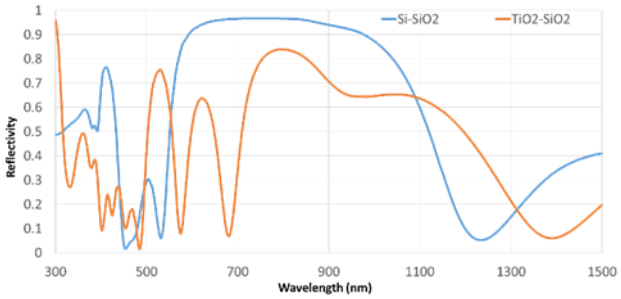

Figure 6: 125 nm, six layers Si-SiO2 and TiO2-SiO2 DBR reflectivity.

3.4. Absorption profile simulation

Towards more optical investigation in the DBR structure optimized in the previous versions, Comsol Multi-physics was utilized. Herein, six layers Si-SiO_2 DBR modeled in the previous section were simulated. The electric field components are used to describe the absorption profile following the Poyting vector method illustrated in [8]. The demonstrated optical absorption profile shown in figure 7, at 550 nm, illustrates the trapping functionality of the DBR structure to trap light inside the active material seeking for optical path length elongation. Accordingly an enhancement of nearly 38% is recorded in the optical generation term. The simulation has been conducted over an optical wavelength range from 200 nm (UV-range) to 2000 nm (IR-range) with a peak at 550 nm.

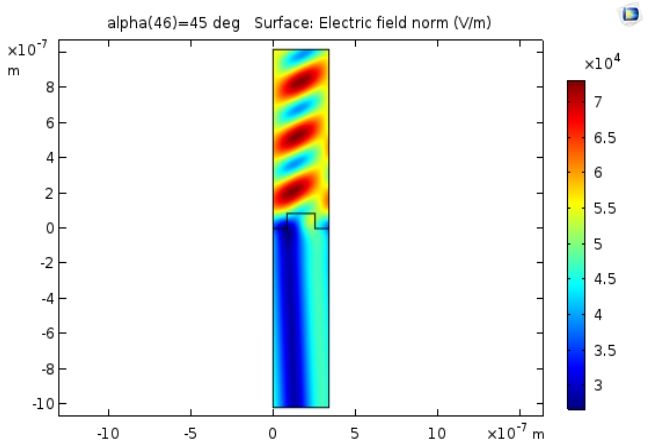

Figure 7: 125 nm, six layers Si-SiO_2 absorption profile.

3.5. Two-dimensional grating light trapping structure

As shown in figure 8a, a 2D grating is characterized as structures that are periodic with a periodicity L in two-dimensions, (e.g. x-direction and y-direction), and are uniform in only one dimension (z-direction). We consider the propagation of incident light in the xz-plane. Since the structure considered is two-dimensional, the reaction of the structures can be separately considered for the s-polarization, which has its electric field polarized along the y-direction, and for the p-polarization, which, as shown in figure 8b, has its magnetic field polarized along y-direction.

With a periodicity L of 1 µm, SiO_2 thickness d_2 of 100 nm, and an aspect ratio (a/b) of 1 (figure 8b), a 2D Si/SiO_2 grating structure is simulated. The minimum x-direction dimension b = 500 nm is used to allow such a device to be fabricated in an area of 200 µm x 200 µm. Furthermore, another experiment was carried out in order to simulate the same structure but with aspect ratio of 2.4. The reflectance of this structure is shown in Figure 9 in the near infrared region with an optical band-gap. With respect to the DBR structure, this shifting in the optical band gap structure is due to the scaling up of the minimum dimension length from 50 nm to 500 nm.

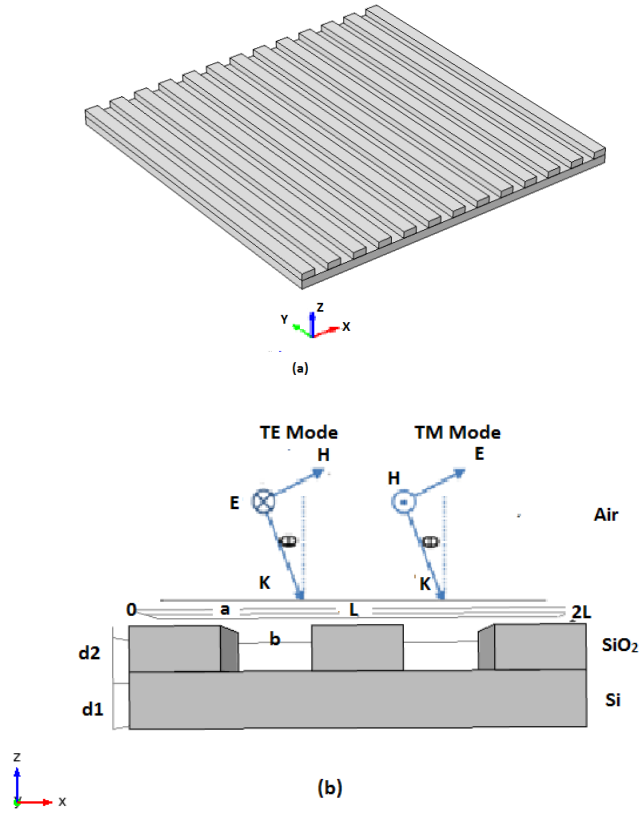

Figure 8: (a) 3D schematic for the structures of 1D grating. (b) X-Z cross section for 1D grating structure.

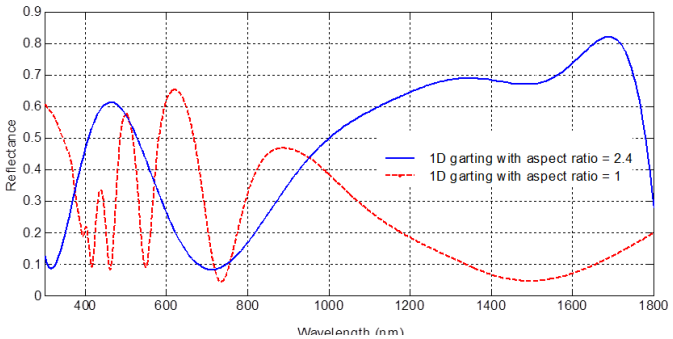

Figure 9: 1D grating structure with aspect ratio of 1 (red curve) and 2.4 (blue curve).

4. Fabrication Process

As mentioned in the introduction, one of our targets here is to fabricate thin film to validate our proposed optical model. Herein, thermal evaporator and spin coater are suggested to be used for this process, while UV-Vis spectrometer is used for the optical characterization purposes.

The thermal evaporator consists of different subsystems. One of the subsystems is the vacuum chamber, the control valves, the vacuum pumps are integrated to satisfy the vacuum itself, and the gauges is utilized to evaluate the pressure level in the chamber. Another obvious subsystem is the filament and the current source required to heat the filament and to control its temperature. Another subsystem measures the thickness of the deposited film so that we can know when the targets are evaporating and when the film deposition is complete. A more trivial subsystem is the framework used physically to hold the substrates and to control whether the evaporated material reaches the substrates.

The Spin coater is equipment enrolled in deposing thin films to flat surfaces substrates. A coating material, usually called suspension, is drooped in the center of the sample before starting the spinning process. The sample is then rotated either in one step or multi-steps with a certain rotating speed and acceleration. This rotation produces the thin film with the aid of centrifugal force.

The speed and the acceleration chosen play an important role in adjusting the thickness of the produced film. The used suspension is usually chosen to be easily evaporated and volatile. It is also worth to mention that not only the speed and acceleration of rotation tune the thickness but also the viscosity and concentration of the suspension. However, in principle, the faster the rotation speeds, the thinner the produced film. Typically, spin coater are used in deposing thin films of few nanometers thick to micrometers range such as the photoresist materials.

For optical characterization, the UV-Vis spectrometer used to scan the ultraviolet to near infrared regions including the visible portion of spectrum. The basic setup of the UV-VIS spectrometer is consisting of a light source which includes two lamps. The first is a tungsten-halogen lamp for the visible and the near infrared (NIR) region. For the UV region, the deuterium lamp is used A NIR and a visible light detector are used in detecting light. Finally, fibers optics cables are used to connect the source detectors and sample holder (cf. Figure 10).

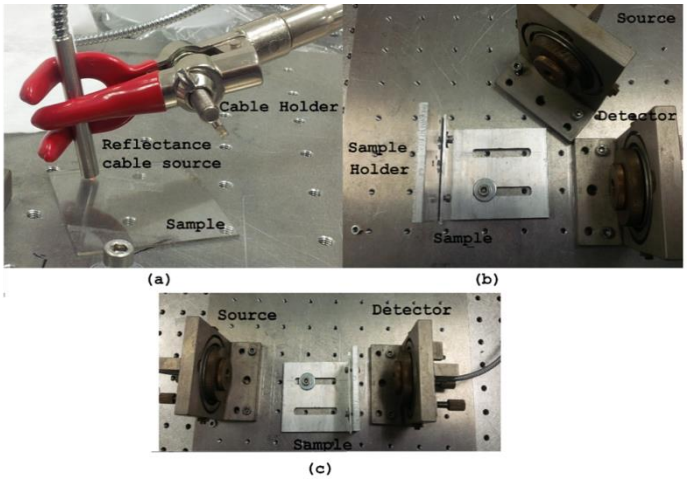

Figure 10: (a) Measuring reflectance using three terminals fibres cable. (b) Measuring reflectance using source/detector setup. (c) Measuring the transmission

5. Experiential validation

In order to validate order optical proposed model, experimental validation take place using thin film based samples. A thermal

evaporation process is used to evaporate a 70 nm of Ag on a highly P-doped Si wafer. The highly P-doped Si wafer is chosen to maintain its optical characteristics during the fabrication process. The thermal evaporation process is done under a current rate of 12% where the tooling factor was previously determined using a dektak profilometer and it was found to be 0.551. The output evaporation rate is 0.1 nm/sec. Then a characterization process takes place using UV-VIS spectrometer to measure the reflectance of the sample in the desired portion of the spectrum as shown in figure 10. The effect of adding the collimating lens is also considered here showing a more accordance with the simulation results than the without collimating lens results. The simulation results shown here are based on our optical numerical model described in the previous section.

The results shown in figure 11 is not only considered as a new validation step to our optical model but it can also be considered as a validation to the new suggested measurement setup of the UV-VIS spectrometer with adding collimating lens. The results show that the adjusted lens doesn't cause any undesirable effect in the wavelength portion of interest making it possible to use such a setup in measuring the reflectance of small area samples.

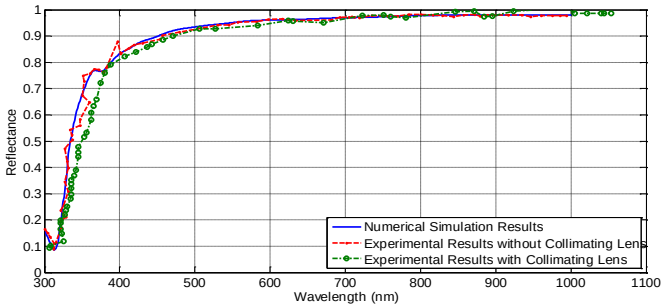

Figure 11: Comparison between the simulated and the measured reflectance of a 70 nm Ag thin film.

A 40 nm thin film of SiO_2 is deposited on a Si <100> wafer using thermal evaporator. The tooling factor is calculated and it was 0.1812 while the current rate is set to be 35%. It is observed that the current needed to evaporate SiO_2 is much higher than that used for Ag, this is due to the high evaporating temperature of SiO_2 with respect to that of Ag. The evaporation rate is varying around 0.01 nm/sec. The Reflectance of the thin film is measured using the UV-VIS spectrometer as observed in figure 12. The figure shows a high accordance between the numerical simulated and the measured reflectance. It was found that due to the high evaporating temperature of SiO_2 (about 1800 ^oC); it is not efficient to evaporate thin film of SiO_2 using thermal evaporation technique. As deposing thin film of SiO_2 must be done by more than one iteration, due to the very low evaporating rate, which causes a poor uniformity of the surface.

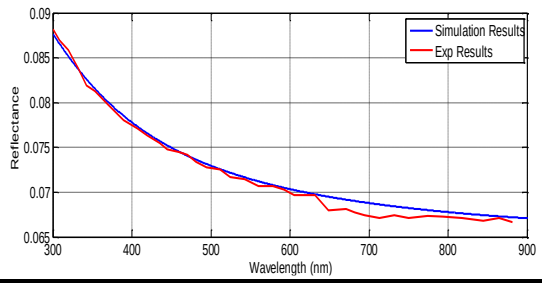

Figure 12: Comparison between the simulated and the measured reflectance of a 40 nm SiO_2 thin film.

It's worth to mention here that the optical validation process implemented on two sample of thin films behaving as optical filter showed perfect agreement with the data captured from our proposed optical model. However, the validation process demonstrated in this paper is limited to thin films samples due to constrain associated with photonic crystals fabrication. Accordingly, we consider the validation step with fabricated photonic crystal structure as a future extension of the current work.

6. Discussions

After the iterations used to optimize DBR structure the output for three steps of optimization that shown in section 3 and also take in consideration the previous measurement in [8], shown in figure 13. By our requested of optimization modal, it is shown the suitable match. Our represented structure is suggested structure to back reflector of thin film of solar cells. This model of structure lead to optical band-gap in near infrared and far visible region, (from 800 nm to 1100 nm) the low absorption occurred at the layer of Si. We attribute such extended band-gap to the refractive index contrast with respect to the DBR shown in figure 5. This structure showed below describe the performance of non-absorbed photons which cannot escape from active layer, after that the light trapping occurred inside material. It is worth to mention that the height (y-axis reflectance value) is inversely proportional to the optical band gap-width [16]. The higher the reflectance the lower the band-gap.

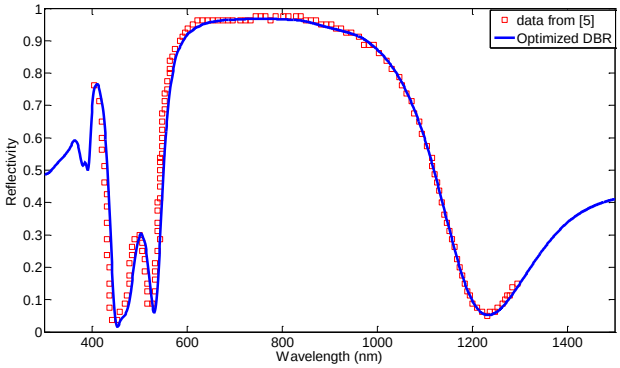

Figure 13: 125 nm, six layers Si-SiO_2 DBR verification with previously published data in [5].

A primary downside within the proposed silicon-slica DBR structure is that the nonappearance of metal which may act as a counter electrode. Consequently, another altered DBR structure with Indium tin-oxide (ITO) rather than Si can be suggested. Though, the proposed planned structure will lack of a condensed optical band-gap because of the less index of refraction distinction with the ITO-SiO_2 DBR with respect to the optimized Si-SiO_2 DBR structure. Additionally, the proposed ITO-SiO_2 DBR structure will show more refined fabrication process, particularly within the deposition of SiO_2 layer the thin ITO layer. Regularly the SiO_2 deposition is achieved by chemical vapor deposition (CVD) at moderately high temperature. Such testimony conditions might influence the ITO electrical properties yet as morphology.

Fundamentally, Nano-lithography technology can be essentially used to fabricate higher dimensions (2D and 3D) photonic crystal structure. In this manner, more refined manufacturing processes and costs would be expected. This specifically influences the cost of delivered energy (Wh/$) by TFSCs. An inclusive analysis showing the effect of the 1D, 2D, and 3D PCs structure in terms of cost versus increase in conversion

efficiency can be carried out as a future task. In principle, alternative low-absorption solar cells can be upgraded using the same light trapping process.

7. Conclusion

The optimization in DBR structure that represented in the paper depends on thickness of layers, refractive index contrast and number of layers. The optimization of DBR structure implement in two step, firstly analytical implantation by MATLAB and secondly verification by using Open-filter. In order to simulate the solar spectrum (AM1.5G), Gaussian sources and FDTD were used.

By using 6 layers of Si-SiO_2 of DBR as result of optimization, the band-gap occurred in 550 nm. This band-gap represents a massive potential in Si as reflected near-infrared of photonics and this reflection avoid light from escaping from material. After comparing between previous data that published and our simulation results, the suitable match was chosen. On another hand, TiO_2 was examined as alternative of Si to observe the effect of changing refractive index in the optical band-gap. At the end the effect of adding metal layer of ITO on Si as substitution was discussed in this paper and released the effect of it on the optical band-gap. Additionally, 2D grating structure was also examined based on the developed optical mode, where transmission spectra were simulated. Fabricated thin films were utilized to validate the optical model while a perfect matching was recorded.

The proposed optical model has showed a great potential in designing optimal 1D and 2D photonic crystal structures with a tunable optical band-gap varying from 400 nm to 700 nm capable of integrating in various solar cells applications. Moreover, the study investigates the optical absorption profile for various photonic crystals seeking for minimum parasitic absorption.

Acknowledgment

In this work, the authors would like to acknowledge the contribution and support of the STDF. As part of the STDF Project entitled, “Mesostructured Based Solar Cells for Smart Building Applications”, Project ID#33502. Additionally, the authors would like to thank the Centre for Emerging Learning Technology (CELT), directed by Prof. Hani Ghali, in BUE for providing all the fabrication facilities needed.

References

[1] S. O. Abdellatif and G. A. Alsayed, "Optimizing 1D Photonic Crystal Structures for Thin Film Solar Cells," in 2019 IEEE Conference on Power Electronics and Renewable Energy (CPERE), 333-337, 2019, doi:10.1109/CPERE45374.2019.8980046.

[2] M. Mujahid, C. Chen, W. Hu, Z.-K. Wang, and Y. Duan, "Progress of High-Throughput and Low-Cost Flexible Perovskite Solar Cells," Solar RRL, 1900556, 2020, doi:10.1002/solr.201900556.

[3] M. Sajadnia, S. Dehghani, Z. Noraeepoor, and M. H. Sheikhi, "Highly improvement in efficiency of Cu (In, Ga) Se2 thin film solar cells," World Journal of Engineering, **17**(4), 527–533 2020, doi:10.1108/WJE-02-2020-0068.

[4] S. Amiri and S. Dehghani, "Design and Simulation of Single-Junction and Multi-junction Thin-Film Solar Cells Based on Copper Tin Sulfide," Journal of Electronic Materials, **49**, 5895–5902, 2020, doi.org/10.1007/s11664-020-08382-6.

[5] F. Sadegh, S. Akin, M. Moghadam, V. Mirkhani, M. A. Ruiz–Preciado, Z. Wang, et al., "Highly efficient, stable and Hysteresis–less planar perovskite solar cell based on chemical bath treated Zn_2SnO_4 electron transport layer," Nano Energy, 105038, 2020, doi:10.1016/j.nanoen.2020.105038.

[6] S. Liu, J. Yuan, W. Deng, M. Luo, Y. Xie, Q. Liang, et al., "High-efficiency organic solar cells with low non-radiative recombination loss and low energetic disorder," Nature Photonics, **14**, 300–305, 2020, doi.org/10.1038/s41566-019-0573-5.

[7] F.-I. Lai, J.-F. Yang, Y.-C. Hsu, and S.-Y. Kuo, "Enhanced omnidirectional light harvesting in dye-sensitized solar cells with periodic ZnO nanoflower photoelectrodes," Journal of Colloid and Interface Science, **562**, 63-70, 2020, doi:10.1016/j.jcis.2019.12.003.

[8] S. Abdellatif, K. Kirah, R. Ghannam, A. Khalil, and W. Anis, "Enhancing the absorption capabilities of thin-film solar cells using sandwiched light trapping structures," Applied optics, **54**, 5534-5541, 2015, doi:10.1364/AO.54.005534.

[9] S. Abdellatif, R. Ghannam, and A. Khalil, "Simulating the dispersive behavior of semiconductors using the Lorentzian–Drude model for photovoltaic devices," Applied optics, **53**, 3294-3300, 2014.

[10] S. Abdellatif and K. Kirah, "Numerical modeling and simulation for a radial pin nanowire photovoltaic device," Energy Procedia, **36**, 488-491, 2013, doi:10.1364/AO.53.003294.

[11] M. M. Hassan, A. Sahbel, S. O. Abdellatif, K. A. Kirah, and H. A. Ghali, "Toward low-cost, stable, and uniform high-power LED array for solar cells characterization," in New Concepts in Solar and Thermal Radiation Conversion III, 114960Q, 2020, doi:10.1117/12.2572874.

[12] G. R. Li and X. P. Gao, "Low-cost counter-electrode materials for dye-sensitized and perovskite solar cells," Advanced Materials, **32**, 1806478, 2020, doi:10.1002/adma.201806478.

[13] B. Pashaei, S. Bellani, H. Shahroosvand, and F. Bonaccorso, "Molecularly engineered hole-transport material for low-cost perovskite solar cells," Chemical Science, **11**, 2429-2439, 2020, doi:10.1039/c9sc05694g.

[14] E. G. Durmusoglu, G. S. Selopal, M. Mohammadnezhad, H. Zhang, P. Dagtepe, D. Barba, et al., "Low-Cost, Air-Processed Quantum Dot Solar Cells via Diffusion-Controlled Synthesis," ACS Applied Materials & Interfaces, **12**, 32, 36301–36310, 2020 doi:10.1021/acsami.0c06694.

[15] J. H. Werner, J. Mattheis, and U. Rau, "Efficiency limitations of polycrystalline thin film solar cells: case of Cu (In, Ga) Se2," Thin Solid Films, **480**, 399-409, 2005, doi:10.1016/j.tsf.2004.11.052.

[16] R. Biswasa and D. Zhoua, "Enhancing Light-trapping and Efficiency of Solar Cells with Photonic Crystals," in Materials Research Sociaty Spring Meeting - Symposium A – Amorphous and Polycrystalline Thin-Film Silicon Science and Technology, Germany, 0989-A03-02, 2007, doi:10.1557/PROC-0989-A03-02.

[17] S. Abdellatif, K. Kirah, R. Ghannam, A. Khalil, and W. Anis, "Comprehensive study of various light trapping techniques used for sandwiched thin film solar cell structures," in Physics, Simulation, and Photonic Engineering of Photovoltaic Devices VII, 10527152018, doi:10.1117/12.2291613.

[18] J. Hou, M. Li, and Y. Song, "Patterned colloidal photonic crystals," Angewandte Chemie International Edition, **57**, 2544-2553, 2017, doi:10.1002/anie.201704752.

[19] W. Zhu, R. Esteban, A. G. Borisov, J. J. Baumberg, P. Nordlander, H. J. Lezec, et al., "Quantum mechanical effects in plasmonic structures with subnanometre gaps," Nature communications, **7**, 1-14, 2016, doi:10.1038/ncomms11495 .

[20] M. Mariano, P. Mantilla-Pérez, P. Romero-Gómez, A. Martínez-Otero, X. Elias, R. Betancur, et al., "One-Dimensional Photonic Crystals for Light Management in Organic Solar Cells," in Organic and Hybrid Photonic Crystals, ed: Springer, 303-320, 2015, doi:10.1007/978-3-319-16580-6_13.

[21] F. Enrichi, A. Quandt, and G. C. Righini, "Plasmonic enhanced solar cells: Summary of possible strategies and recent results," Renewable and Sustainable Energy Reviews, **82**, 2433-2439, 2018, doi: 10.1016/j.rser.2017.08.094.

[22] C. Zhao, P. Tong, L. Shi, T. Ji, F. Zhu, Y. Hao, et al., "Performance improvement in inverted organic solar cells by incorporating core-shell SiO_2@ Au plasmonic structures," in 9th International Symposium on Advanced Optical Manufacturing and Testing Technologies: Micro-and Nano-Optics, Catenary Optics, and Subwavelength Electromagnetics, 108400N, 2019, doi:10.1117/12.2510899.

[23] R. S. Moakhar, S. Gholipour, S. Masudy-Panah, A. Seza, A. Mehdikhani, N. Riahi-Noori, et al., "Recent Advances in Plasmonic Perovskite Solar Cells," Advanced Science, **7**, 1902448, 2020, doi:10.1002/advs.201902448.

[24] J. D. Joannopoulos, P. R. Villeneuve, and S. Fan, "Photonic crystals: putting a new twist on light," Nature, **386**, 143-149, 1997, doi:10.1038/386143a0.

[25] A. Fu, H. Gao, P. Petrov, and P. Yang, "Widely tunable distributed Bragg reflectors integrated into nanowire waveguides," Nano letters, **15**, 6909-6913, 2015, doi:10.1021/acs.nanolett.5b02839.

[26] S.-P. Yu, J. A. Muniz, C.-L. Hung, and H. Kimble, "Two-dimensional photonic crystals for engineering atom–light interactions," Proceedings of

the National Academy of Sciences, **116**, 12743-12751, 2019, doi: 0.1073/pnas.1822110116.
[27] S. Abdellatif, S. Josten, P. Sharifi, K. Kirah, R. Ghannam, A. S. Khalil, et al., "Optical investigation of porous TiO_2 in mesostructured solar cells" 10526: SPIE, 2018, doi:10.1117/12.2288376.
[28] S. Abdellatif, P. Sharifi, K. Kirah, R. Ghannam, A. Khalil, D. Erni, et al., "Refractive index and scattering of porous TiO_2 films," Microporous and Mesoporous Materials, **264**, 84-91, 2018, doi: 10.1016/j.micromeso.2018.01.011.
[29] S. O. Abdellatif, S. Josten, A. S. Khalil, D. Erni, and F. Marlow, "Transparency and Diffused Light Efficiency of Dye-Sensitized Solar Cells: Tuning and a New Figure of Merit," IEEE Journal of Photovoltaics, **10**, 522-530, 2020, doi:0.1109/JPHOTOV.2020.2965399.
[30] S. Kamal, G. M. Al-sayyad, R. Abdelmoteleb, M. Abdellatif, and S. O. Abdellatif, "Submerged Solar Energy Harvesters Performance for Underwater Applications," in 2019 International Conference on Innovative Trends in Computer Engineering (ITCE), 444-449, 2019, doi:10.1109/ITCE.2019.8646459..
[31] M. M. Abdellatif, S. M. Maher, and M. Ghazal, "Implementation of a low cost, solar charged RF modem for underwater wireless sensor networks," International Journal on Smart Sensing and Intelligent Systems, **13**, 1, 1-11, doi:10.21307/ijssis-2020-015.
[32] S Larouche and L Martinu, "OpenFilters: open-source software for the design, optimization, and synthesis of optical filters," Appl. Opt. **47**, C219-C230, 2008, doi:10.1364/AO.47.00C219.
[33] E. Hecht, OPTICS, Fourth eddition. Adelphi university, San Francisco, Boston, New York, 2002.
[34] A. D. Rakić, A. B. Djurišić, J. M. Elazar, and M. L. Majewski, "Optical properties of metallic films for vertical-cavity optoelectronic devices," Applied optics, 37, 5271-5283, 1998, doi:10.1364/AO.37.005271.
[35] K. Kunz and R. Luebbers, Finite differnce time domain method for electromagnatics. United State of America: CRC Press, 1993.
[36] J. D. Joannopoulos, "MEEP," ed: Massachusetts Institute of Technology, https://meep.readthedocs.io/en/latest/, accessed October 2020.
[37] A. F. Oskooi, D. Roundy, M. Ibanescu, P. ermel, J. D. Joannopoulos, and S. G. Johnson, "Meep: A flexible free-software package for electromagnetic simulations by the FDTD method," Computer Physics Communications, ELSEVER, **181**, 687–702, 2010, doi:10.1016/j.cpc.2009.11.008.
[38] "Reference solar spectral irradiance: Air mass 1.5," ed: National Renewable Energy Lab.
[39] C. Multiphysics, "version 4.2," Heat Transfer Module, https://www.comsol.com/products/4.2/, accessed October 2020.